

Uncertainty quantification in Eulerian-Lagrangian simulations of (point-)particle-laden flows with data-driven and empirical forcing models

Vasileios Fountoulakis^a, H.S. Udaykumar^b, Gustaaf B. Jacobs^a

^a*Department of Aerospace Engineering, San Diego State University, San Diego, CA*

^b*Department of Mechanical and Industrial Engineering, The University of Iowa, Iowa City, IA*

corresponding author, gjacobs@sdsu.edu

July 2, 2019

Abstract

An uncertainty quantification framework is developed for Eulerian-Lagrangian models of particle-laden flows, where the fluid is modeled through a system of partial differential equations in the Eulerian frame and inertial particles are traced as points in the Lagrangian frame. The source of uncertainty in such problems is the particle forcing, which is determined empirically or computationally with high-fidelity methods (data-driven). The framework relies on the averaging of the deterministic governing equations with the stochastic forcing and allows for an estimation of the first and second moment of the quantities of interest. Via comparison with Monte Carlo simulations, it is demonstrated that the moment equations accurately predict the uncertainty for problems whose Eulerian dynamics are either governed by the linear advection equation or the compressible Euler equations. In areas of singular particle interfaces and shock singularities significant uncertainty is generated. An investigation into the effect of the numerical methods shows that low-dissipative higher-order methods are necessary to capture numerical singularities (shock discontinuities, singular source terms, particle clustering) with low diffusion in the propagation of uncertainty.

1 Introduction

Particle-laden flows occur in a number of engineering applications and natural environments, including aerosol and sprays flows in combustion engines and

medical devices, dispersion of environmental pollutants, etc. In some applications the carrier gas flow travels at high/supersonic speed and shock waves interact with the particles. Some examples are the dynamics in scramjet combustors, detonation of explosives, and volcanic eruptions.

The number of particles in a process-scale environment is too large to model with first-principles models. Macro-scale models and simulation techniques are necessary to simulate such problems. An Eulerian-Lagrangian (EL) approach combined with point-particle modeling is commonly used to make computations more efficient. In these EL models, the carrier flow is solved in the Eulerian frame, while the volumeless particles (Particle-Source-In-Cell, or PSIC) are traced along their Lagrangian path [1]. The interactions between the particles and the carrier fluid are modeled through momentum exchange via singular point source terms [2, 3].

These point particle approaches require a model for the drag force exerted on the particles. Under the assumptions of very low Reynolds number, incompressible flow and spherical particles an analytical solution exists: the Stokes drag law [4]. For high Reynolds numbers several empirical laws have been developed. These laws correct the Stokes drag law for various effects: compressibility [5, 6], slip coefficients [7], viscosity ratio for droplets [8], and others. Generally, physical experiments, canonical theoretical constructs, and phenomenological arguments are employed to obtain expressions for the drag forces. A drawback of empirical expressions is the limited range in parameter space.

In an ongoing effort, we address this limitation through multi-scaling. We use resolved mesoscale simulations to derive drag force models in a range that applies to an arbitrary macro-scale parameter range [9, 10]. This is achieved by construction of data-driven metamodels from a limited amount of data for drag laws, heat transfer, particle-fluid correlations etc. over a wide range of parameters such as the Mach number, Reynolds number, and particle phase number density.

Both empirical models and meta-models have associated uncertainties, arising from measurement, numerical errors and sparsity of the data points. To understand how this model uncertainty affects the solution on the macro-scale, one must understand how uncertainty propagates through the non-linear Eulerian-Lagrangian model. This understanding begins by using a probabilistic perspective and by modeling the drag force as a random variable. The quantities of interest (QoIs), such as the flow dynamics and particle dispersion and mixing, are greatly influenced by the epistemic uncertainty in the drag forces. As a consequence, the QoIs have to be modeled as random variables also. This yields a classic stochastic formulation that requires techniques from the field of uncertainty quantification (UQ).

A proper and complete description of the random variables is through the estimation of the probability density function, since our quantities of interest are continuous random variables. To this end, deterministic equations for the evolu-

tion of the probability density function of the quantities of interest for advection-reaction equations were developed [11]. Cumulative density function evolution equations of the QoIs for kinematic wave equations have been developed in [12]. However, these methods remain to be extended to systems involving singularities, such as shocks propagating through a multiphase mixture with singular sources.

One of the classic approaches quantifying uncertainties is Monte Carlo (MC). Even though MC is easy to implement, convergence requires many samples that makes the method computationally inefficient. Other variants of MC methods that employ more advanced sampling techniques e.g. Latin hypercube sampling [13] and multilevel MC [14] partially mitigate this difficulty.

The stochastic finite element method (SFEM) is a different approach that has been used for UQ tasks [15]. It is based on the expansion of the QoIs on the stochastic space using orthogonal polynomials of the random variables (generalized polynomial chaos (gPC) [16]). Another variant of gPC, the multi element generalized polynomial chaos method, was introduced to deal with the discontinuities in the stochastic space [17, 18]. However, both methods suffer from their intrusive nature (having to modify the deterministic code and ending up with a high-dimensional coupled system of equations) and the curse of dimensionality.

In order to deal with the intrusive nature of SFEM researchers proposed stochastic collocation methods [19]. Some of these methods, i.e. adaptive sparse grid collocation [20], are able to deal with discontinuities in the stochastic space successfully. In addition, Gaussian processes [21] have been also employed to develop a Bayesian UQ framework that is based on surrogates models [22].

In this paper, we develop a model that propagates the uncertainty of the drag force through a non-linear coupled EL system. The approach is based on the averaging of the governing equations and allows for an estimation of the first moments of uncertainty. The main advantage of the proposed framework is the simplicity, accuracy, and the computational efficacy. This efficiency becomes particularly important when a feedback loop is used to reduce the uncertainty in the surrogate models based on uncertainty in the QoI, a natural extension of the current work. In that case, iterations between the QoI and the drag surrogate model are required that use the computational intensive stochastic macro-models to reduce the uncertainty in the system. A downside of averaging procedures is that the final system of equations is not closed. We handle the closure problem a priori by using simulated data. In future efforts, a more consistent a posteriori closure will be sought.

We demonstrate that within this UQ framework only two moments are required to accurately predict the uncertainty for problems governed by linear advection and the compressible Euler equations in Eulerian frame. We also report on the effect of numerical approximation, shock discontinuities, singular source terms and particle clustering on the propagation of uncertainty.

The paper is organized as follows. In Section 2, the deterministic equations

for the Euler equations and the linearized problems are presented. In Section 3, we derive the stochastic equations. In Section 4, we briefly summarize the numerical methods employed for the solution of the equations. Numerical tests and discussion of the results are presented in Section 5. Conclusions and future research directions are drawn in the Section 6.

2 Deterministic models

We adopt the EL model with the carrier phase governed by the compressible Euler equations in the Eulerian frame. This system poses several challenges in terms of mathematical modeling and numerical predictions. Discontinuous solutions exist because of the presence of the shocks. In addition, the treatment of the particles as mathematical points leads to the appearance of singular source terms in the conservation of momentum. These characteristics of shock particle-laden flows also present stiff challenges to a UQ framework. To test and verify the UQ framework, we consider simplifications in the following aspects: a) using 1D models, b) linearization of the Eulerian equations and c) smoothing of the singular particle source terms. In the following we present the coupled equations that describe the dynamics of the fluid flow and the kinematic and dynamic equations that govern the particle motion.

2.1 Deterministic Eulerian-Lagrangian Equations

The compressible inviscid flows are governed by the Euler equations which in one-dimensional conservative form are given by:

$$\frac{\partial \mathbf{Q}}{\partial t} + \frac{\partial \mathbf{F}}{\partial x} = \mathbf{S} \quad (1)$$

where

$$\mathbf{Q} = [\rho, \rho u, E]^T, \quad (2a)$$

$$\mathbf{F} = [\rho u, \rho u^2 + P, (E + P)u]^T, \quad (2b)$$

$$\mathbf{S} = [0, S_m, S_e]^T \quad (2c)$$

where ρ is the density of the fluid, u is the velocity of the fluid, E is the energy of the fluid and P is the pressure and given by $P = (\gamma - 1) (E - \rho u^2/2)$, $\gamma = 1.4$. These equations are closed by the equation of state $T = \gamma P M^2 / \rho$, where $M = U / \sqrt{\gamma R T}$ is a reference Mach number determined with the reference velocity (U) and reference temperature T . The source terms in equation (2c) are given

by

$$S_m = \sum_j^{N_P} f_1 \frac{m_p}{\tau_p} (u_{p_j} - u) \delta(x - x_{p_j}), \quad (3a)$$

$$S_e = \sum_j^{N_P} \left(f_1 \frac{m_p}{\tau_p} (u_{p_j} - u) u_{p_j} + f_2 \frac{m_p}{\tau_p} (T_{p_j} - T) \right) \delta(x - x_{p_j}) \quad (3b)$$

where T is the fluid temperature, N_p is the number of particles, τ_p is the particle time constant, m_p is the particle mass, u_{p_j} is the particle velocity, x_{p_j} is the particle position, T_{p_j} is the particle temperature, f_1 and f_2 are correction factors. The factor $f_2 = Nu/(3Pr)$ is determined by the Nusselt number (Nu) and the Prandtl number (Pr). The empirical correction factor f_1 is given by the expression [23] :

$$f_1 = (18 + 0.285Re_p + 3\sqrt{Re_p}) \left(1 + \exp \left[-\frac{0.43}{M_f^{4.67}} \right] \right) \quad (4)$$

where Re_p is the relative particle Reynolds number and M_f is the relative particle Mach number. This correction factor is again our source of uncertainty in the system and is treated as a random variable later on.

The particles are tracked in the Lagrangian frame. Position of the particles is given by

$$\frac{dx_p}{dt} = u_p \quad (5)$$

The particle velocity is given by Newton's second law. The drag force is a combination of the corrected Stokes law for high Reynolds and Mach number and the pressure drag [23]:

$$\frac{du_p}{dt} = f_1 \frac{u - u_p}{\tau_p} - \frac{1}{\rho_p} \frac{\partial P}{\partial x} \quad (6)$$

where ρ_p is the density of the particles. Finally, the particle temperature is calculated from the Fourier's law of heat transfer and the first law of thermodynamics:

$$\frac{dT_p}{dt} = f_2 \frac{T - T_p}{\tau_p} \quad (7)$$

2.2 Advection equation

For the purpose of verification and testing, we have considered a linear advection equation for an Eulerian model whose solutions do not contain the challenging non-linear behavior of the compressible Euler equation. This allowed us to focus on the coupling between the Eulerian and Lagrangian system. We performed

tests using the linear advection equation in 1D for the Eulerian model with a particle interaction source term as follows:

$$\frac{\partial u}{\partial t} + \frac{\partial u}{\partial x} = S_m. \quad (8)$$

The particles are tracked individually in their Lagrangian frame. The position of the particle (x_p) is given by equation (5). The velocity of the particle is determined by Newton's second law forced by the drag on the particle:

$$\frac{du_p}{dt} = f_1 \frac{u - u_p}{\tau_p} \quad (9)$$

These equations form a system of coupled equations with linear advection behavior and are similar to the coupled system of Euler equations with particles.

3 Stochastic models

We use a corrected Stokes law for high Reynolds and Mach numbers to calculate the drag force exerted on the particles. This drag law is an empirical law, therefore subject to uncertainty. To simulate the uncertainty of this calculation we will treat the empirical correction factor (f_1) as a random variable. This uncertainty is propagated to the fluid and particles QoIs, which are treated as random variables as well.

In the following, we derive the equations for the first couple of moments for the linear advection and the Euler equations based on the Reynolds and Favre average procedures respectively.

3.1 Advection equations

Using Reynolds averaging we derive equations for the first two moments of the EL system based on linear advection equation. The instantaneous value is decomposed as $u = \bar{u} + u'$, where \bar{u} is the mean field and u' is the fluctuation. The stochastic equations derived for the linear advection equation are the following:

$$\frac{\partial \bar{u}}{\partial t} + \frac{\partial \bar{u}}{\partial x} = \overline{S_m}, \quad (10a)$$

$$\frac{\partial \sigma_u}{\partial t} + \frac{\partial \sigma_u}{\partial x} = 2\overline{uS_m} - 2\bar{u}\overline{S_m} = 2\overline{S_m u'} \quad (10b)$$

where $\overline{(\cdot)}$ denotes the Reynolds averaged quantity and $\sigma_{(\cdot)}$ is the variance of the quantity. To obtain an equation for the variance we used the identity:

$\sigma_u = \overline{u^2} - \bar{u}^2$. Similarly, we derive the particle stochastic equation as follows:

$$\frac{\partial \bar{x}_p}{\partial t} = \bar{u}_p, \quad (11a)$$

$$\frac{\partial \sigma_{x_p}}{\partial t} = 2\bar{x}_p \bar{u}_p - 2\bar{x}_p^2 \bar{u}_p, \quad (11b)$$

$$\frac{d\bar{u}_p}{dt} = f_1 \frac{\overline{u - u_p}}{\tau_p}, \quad (11c)$$

$$\frac{\partial \sigma_{u_p}}{\partial t} = 2f_1 \bar{u}_p \frac{\overline{u - u_p}}{\tau_p} - 2\bar{u}_p f_1 \frac{\overline{u - u_p}}{\tau_p} \quad (11d)$$

3.2 Euler equations

In compressible flows, Favre averaging is the most common way to obtain moment equations. Favre averaging $u = \tilde{u} + u''$ is a density-weighted variant of the Reynolds averaging where the mean field is $\tilde{u} = \overline{\rho u} / \bar{\rho}$. The mean field equations are the following:

$$\frac{\partial \bar{\rho}}{\partial t} + \frac{\partial \bar{\rho} \tilde{u}}{\partial x} = 0 \quad (12a)$$

$$\frac{\partial \bar{\rho} \tilde{u}}{\partial t} + \frac{\partial (\bar{\rho} \tilde{u}^2 + \bar{P})}{\partial x} = \bar{S}_m - \frac{\partial \overline{\rho u''^2}}{\partial x} \quad (12b)$$

$$\frac{\partial \bar{E}}{\partial t} + \frac{\partial (\bar{E} + \bar{P}) \tilde{u}}{\partial x} = \bar{S}_e - \frac{\partial (\overline{E + P}) u''}{\partial x} \quad (12c)$$

where $\tilde{(\cdot)}$ denotes the Favre-averaged quantities.

Here, our focus is on the fluid velocity as a QoI. A measure of the velocity uncertainty comes from its second moment, which in our case is $\overline{u''^2}$. This quantity is related to the turbulence kinetic energy, $k = \overline{u''^2} / 2$, which is governed by the following equation:

$$\frac{\partial k}{\partial t} + \tilde{u} \frac{\partial k}{\partial x} = -2k \frac{\partial \tilde{u}}{\partial x} - \frac{1}{2\bar{\rho}} \frac{d}{dx} \overline{\rho u''^3} - \frac{1}{\bar{\rho}} \frac{\partial \bar{P}}{\partial x} u'' + \frac{1}{\bar{\rho}} \overline{S_m u''} \quad (13)$$

All the equations above have terms that include the expected value of the product of two or more quantities. For example, the source term \bar{S}_m when averaged using (3) leads to:

$$\bar{S}_m = \sum_j^{N_P} \frac{m_p}{\tau_p} (f_1 (\overline{u_{p_j} \delta(x - x_{p_j})} - \overline{u} \delta(x - x_{p_j})) + \overline{f_1' u_{p_j}' \delta(x - x_{p_j})} + \overline{f_1' u' \delta(x - x_{p_j})}) \quad (14)$$

Terms such as the last two terms in the equation above are in general not known a priori so the system of equations is not closed. To test averaged equations

it is common to use a posteriori closure. In this study, we choose to follow this approach and determine the closure terms from data that are gathered for different realizations of the correction factor f_1 . In future work, we aim to use a multi-scale framework to provide us with a closed system of equations that can be used for uncertainty quantification purposes. Here, we focus on the formulation and testing of the averaged governing system of equations.

While the equations appear fairly straightforward, there are a number of characteristics of the governing system of equations that pose challenges for solving them. We remark on them below:

Remark 1

The Dirac distribution function in the deterministic term is singular. If there are isolated particles or clusters of particles in the particle-phase where the particle number density suddenly changes, then the deterministic source term can be singular also. To regularize these a number of techniques exist [24, 25].

Remark 2

The averaged source term $\overline{S_m}$ is the sum of the deterministic source terms in equation (3). A singular deterministic source term can make the averaged source term singular or near singular as well. To accurately capture it sufficient resolution and large number of samples are required.

Remark 3

Shock singularities in the fluid phase create near-singular averaged source terms also. The derivatives on the right hand side in equation (13) are near-singular in shock regions where the pressure, velocity and other fluid variables are discontinuous. These need to be regularized.

Remark 4

Two well-known particle-phase dynamics and dispersion patterns include trajectory crossing where two particles have significantly different velocity at the same location and particle clustering, where particles accumulate in a small area. Both these effects lead to singularities in the moments and/or difficulties in determining and closing the moments [26].

Remark 5

The variance equations include directly or indirectly the variation of the realizations (u' or u'') of the fluid phase solution. In regions where the deterministic solution is singular, the variance of the stochastic solution is inherently large and singular. This affects the right hand side in equation equation (13) and the source term in equation equation (10).

4 Numerical Approximations

To solve the governing EL system in section 2.1, we employ the Particle-Source-In-Cell (PSIC) method [1, 2]. In this method, the Eulerian models are approximated on a static grid, while the point particles are traced on a Lagrangian frame. The influence of the point particle on the carrier phase is distributed over the grid through distribution functions, while the influence of the carrier phase is interpolated to the particle position.

Initially, we approximate the advection equation equation (8) and the stochastic linear equations equation (10) with a simple first-order upwind scheme on a uniform mesh in space and temporally with the first-order explicit Euler scheme. To verify the solution of equation (10), we perform MC simulations. From the realizations of the MC simulations we determined the closure source terms a priori and substituted them in the stochastic equation equation (8), which could then be solved.

Despite the usage of significant resolution, we find that the combination of the lower-order upwind schemes lead to significant numerical diffusion near singular sources in the solution of the stochastic equation and the match with MC is poor.

We subsequently solve the deterministic and stochastic linear advection equation using the Chebyshev collocation method [27] in space. For the time discretization we used a fourth-order Runge-Kutta method. As compared to the first-order schemes this reduced the dissipation significantly and lead to a much better match between the MC results and the method of moments.

For the solution of the Euler equations we used the high-order Weighted - Essentially - Non - Oscillatory (WENO-Z) based PSIC algorithm that is described in detail in [2].

Particle tracking requires a three stage algorithm: 1) locate the host cell of the particle, 2) interpolate the fluid variables to the particle location, and 3) time advance with a time integration method. To determine the influence of the particles on the static grid that is used to solve the carrier fluid equation, we must approximate the delta function ($\delta(x)$). A normalized distribution function

is used to distribute the influence of the particles onto the carrier fluid. Here we use either a higher-order spline or a Gaussian distribution function.

To avoid aliasing errors the order of interpolation of the fluid quantities at the particle location must match that of the fluid solver [28]. Hence, we use a fifth-order essential non-oscillatory (ENO) interpolation that is tailored for flows containing shock discontinuities [2]. In addition, a fifth-order spline [29] is employed to weight the contribution of the particles onto the fluid solver grid.

5 Tests

To verify the moment equations and understand the propagation of the uncertainty in the coupled EL system we first focus on an EL system whose Eulerian dynamics are governed by a linearized advection equation. We subsequently test our framework with the full nonlinear EL system.

5.1 Advection equation with a single particle

We begin by taking the source term to be a single smooth exponential function to avoid singularity issues as described in the Remarks above:

$$S_m = -\frac{m_p f_1(u - u_p)}{\tau_p \sqrt{2\pi\sigma_\delta^2}} \exp\left[-\frac{(x - x_p)^2}{2\sigma_\delta^2}\right], \quad (15)$$

where σ_δ^2 controls the spread of the exponential function. We use a single particle to track the peak of this exponential function and the kinematic equations for this particle is given by equation (5) and equation (9).

The domain is set up as $x \in [0, 0.07]$. Periodic boundary conditions are imposed on the boundaries of the domain. The particle response time and the total mass of the particles are: $\tau_p = 0.01$ and $m_p = 0.002$ respectively.

First, we performed computations with the first-order upwind scheme. The grid spacing is $\Delta x = 1e - 5$ and the time step is obeying the CFL condition $\Delta t = 0.4\Delta x$. The length scale of the exponential function is set to one hundred times the grid spacing $\sigma_\delta = 10^{-3}$. We initialize the particle at $x_p = 0.02$ at rest. Finally, we assume that the correction factor follows a Gaussian distribution with a twenty percent error $f_1 \sim \mathcal{N}(1, 0.2)$.

We take the MC solution to be the ground truth and compare the results of moment equations with them. We are able to predict accurate uncertainty bounds (mean value plus and minus two standard deviations) as shown in Figure 1 through Figure 3.

Initially, at the particle location the velocity difference between the particle and fluid causes the source term to be negative. This results in sudden reduction

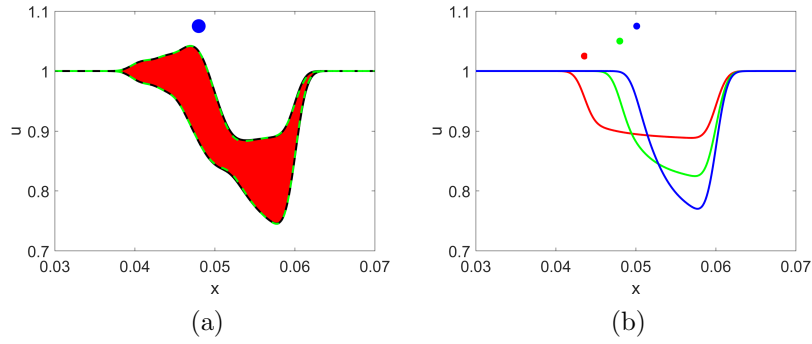


Figure 1: (a) Two standard deviation uncertainty bounds for the fluid velocity. The computational particle location is depicted by the blue dot. Red region and the black lines correspond to the method of moment results and the green dashed line to corresponds to MC results. (b) The fluid velocity (solid lines) for three different values of the correction factor ($f_1 = 0.6$ (red), 1(green), 1.4(blue)) and their corresponding particle position (dots).

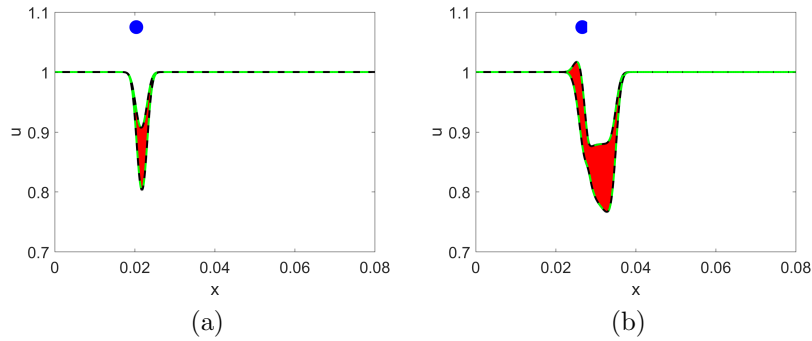


Figure 2: Two standard deviation uncertainty bounds for the fluid velocity. The computational particle location is depicted by the blue dot. Red region and the black lines correspond to the method of moment results and the green dashed line to corresponds to MC results.

in fluid velocity (u) at the initial particle position. This jump in fluid velocity (u) is advected away from the particle location at the advection velocity (in our case unity), because the inertia of the particle yields a lower particle velocity than this advection velocity. At later times the particle velocity catches up. A second jump in fluid velocity (u) coincides with the particle location and the associated inherent sourcing in the advection equation. As the particle catches up with the advection velocity, the sourcing and fluid velocity (u) jump reduces. Over time this results in the formation of a well like the one shown in Figure 1b.

Changes in the magnitude of the correction factor in equation (4) effectively change the response time of the particle. This subsequently controls the well width and particle location as shown in Figure 1b. Initially, the uncertainty is localized at the particle location (Figure 2a) and is advected over time according to equation (10)b. At later times, the uncertainty has two maxima: the boundaries of the well in fluid velocity (u). There, the solutions for different correction factors are significantly different as follows from Figure 1b and therefore cause a high uncertainty. In the area between the boundaries of the well, we notice in Figure 1b that the realizations of the solutions are closer to each other, which results in a region of relatively lower uncertainty.

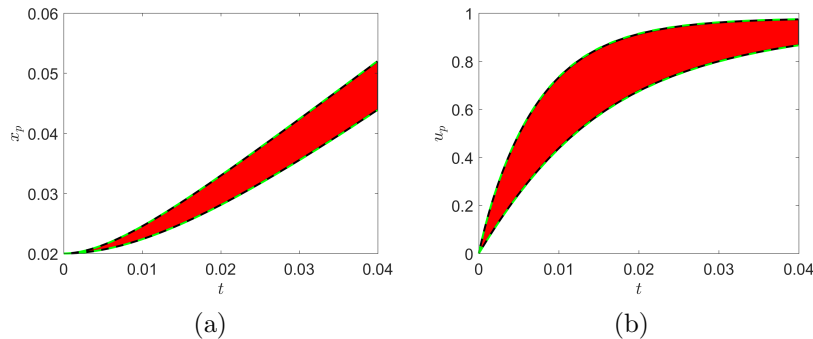


Figure 3: Red region and the black lines correspond to the method of moment results and the green dashed line to corresponds to MC results. (a) Two standard deviation uncertainty bounds for the particle position. (b) Two standard deviation uncertainty bounds for the particle velocity.

The moment equations accurately predict the uncertainty of the particle quantities (Figure 3). The particle position uncertainty keeps increasing with time. The particle velocity uncertainty increases with time at the initial stages of the simulation. Eventually, the particle velocity matches fluid velocity (u) so the uncertainty decreases at later times. With shorter response times (i.e. a larger correction factor), the time interval over which the particle velocity asymptotically matches the fluid velocity (u) reduces, which explains the trends of the upper and lower bound and the uncertainty in Figure 3b.

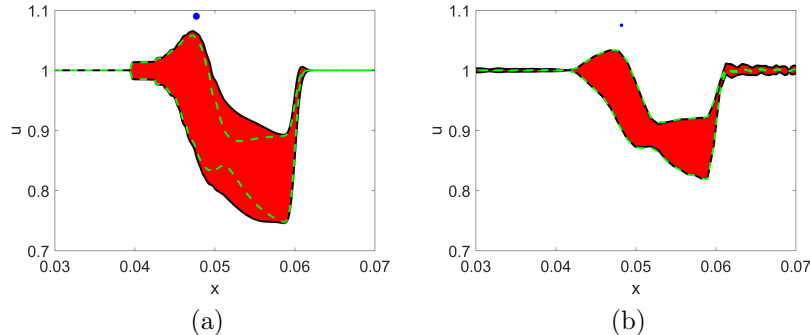


Figure 4: Red region and the black lines correspond to the method of moment results and the green dashed line to corresponds to MC results. Two standard deviation uncertainty bounds for the fluid velocity. The computational particle location is depicted by the blue dot. (a) using first-order methods (b) using high-order methods

If we reduce the support of the exponential source term, then the first-order method no longer shows a good match between MC and the method of moments. If we take the width of the Gaussian distribution function to be 10 times the grid spacing, $\sigma_\delta = 10\Delta x$, then the mean value, \bar{u} , is predicted accurately. However, there is a clear inaccuracy in the prediction of the uncertainty in figure 4a. In equation (10) we notice that the right hand side depends on the source term (S_m) and the variation (u'). By reducing the support of the exponential distribution function, we create a more singular source term but the numerical method is able to overcome this difficulty and capture the expected value accurately. Since we have an inaccuracy in the estimation of the second moment only, we conclude that the source of this inaccuracy is the high variation of (u') as explained in Remark 5. For the case with the larger support width, the solution is much smoother and does not cause the variation to be nearly singular.

First-order methods are very diffusive and not very accurate for such problems so we solve the equations with high-order method as well. We report the result obtained in figure 4b. The high-order method solves the inaccuracy problem and captures accurately the uncertainty. A slight dispersive error common for high-order method solution with sharp gradients shows in the form of oscillations in the far field. This is much less of a concern than the significant diffusive errors of the upwind solution.

5.2 Advection equation with multiple particles

Now we consider the advection equation using multiple particles. We use 1601 particles, which are initialized in $[0.01, 0.0132]$ uniformly at rest. The mass of the particles is set to be $m_p=0.002$. To be consistent with the accuracy of the

space discretization we use linear interpolation to calculate the fluid properties at the grid location. In addition, a first-order distribution function (tent spline) is employed to distribute the particle influence onto the two closest grid points.

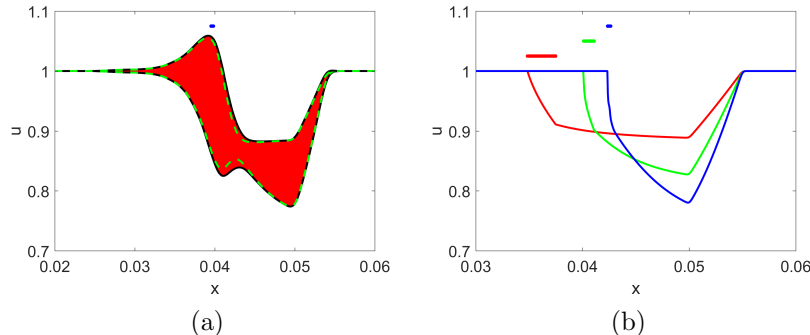


Figure 5: (a) Two standard deviation uncertainty bounds for the fluid velocity. The computational particle location is depicted by the blue dot. Red region and the black lines correspond to the method of moment results and the green dashed line to corresponds to MC results. (b) The fluid velocity (solid lines) for three different values of the correction factor ($f_1 = 0.6$ (red), 1(green), 1.4(blue)) and their corresponding particle position (dots).

The moment equations predict uncertainty bounds that closely match MC results as shown at Figure 5 and Figure 6. The behavior of the solution and uncertainty bounds closely follow the single exponential source case. This is not surprising since the cumulative effect of the multiple particle is a relatively smooth sourcing with a wide support.

One interesting feature of the multiple particles case is that the particle trajectories cross, i.e. the particles initially located at the front of the cloud overtake the particles that are initially located at the rear end of the cloud. This can be explained as follows. Initially, the front of the cloud faces the field, u , and reduces its value through its inertial source, thereby shielding the rear of the cloud. As time advances the particles with higher velocity keep accelerating more and eventually pass particles that are at the rear of the cloud.

The trajectory crossing affect the uncertainty distribution in the particle cloud. We report the variance of the particle position for each particle in the cloud in Figure 7. We index them from left to right as they are oriented in the initial configuration. At initial times the front of the cloud experiences higher uncertainty because of its greater forcing till the trajectory crossing occurs. At the trajectory crossing time, particles are practically at the same location and the uncertainty is uniformly distributed along the particles. After the trajectory crossing, the initial rear of the cloud (higher index number) has become the front of the cloud. Therefore, it experiences higher incoming fluid velocity (u) field resulting in relatively higher uncertainty for those particles.

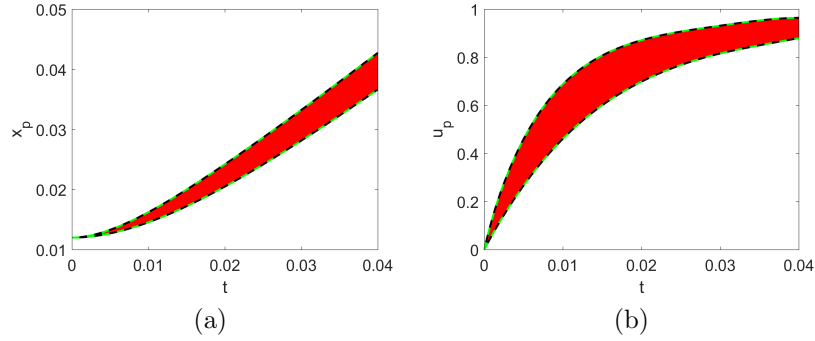


Figure 6: Red region and the black lines correspond to the method of moment results and the green dashed line to corresponds to MC results. Both plots correspond to a particle in the middle of the cloud. (a) Two standard deviation uncertainty bounds for the particle position. (b) Two standard deviation uncertainty bounds for the particle velocity.

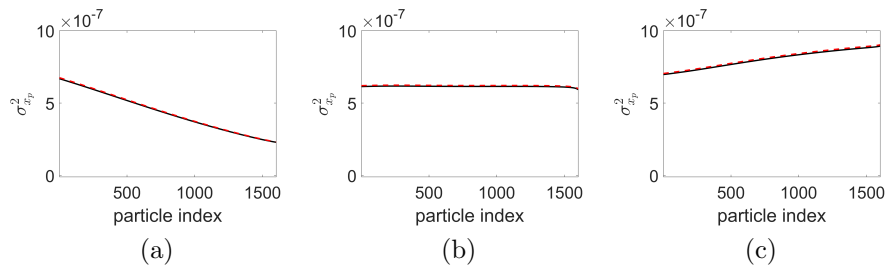


Figure 7: Variance of the particle velocity for the cloud at three different times: a) before trajectory crossing, b) at trajectory crossing, c) after trajectory crossing.

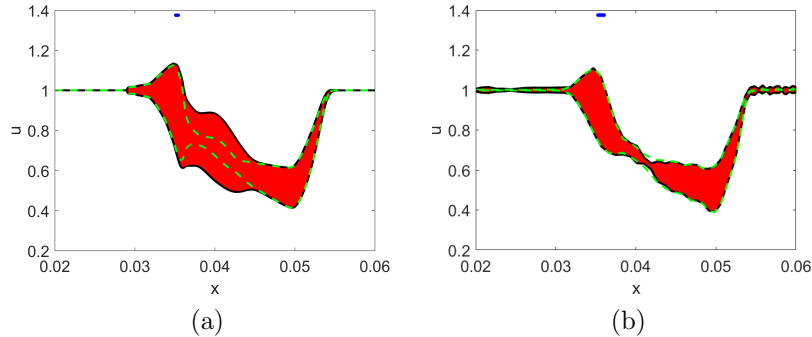


Figure 8: Red region and the black lines correspond to the method of moment results and the green dashed line to corresponds to MC results. Two standard deviation uncertainty bounds for the fluid velocity. The computational particle location is depicted by the blue dot. (a) using first-order methods (b) using high-order methods

Changing the mass of the particles has a significant effect on the accuracy of the predicted uncertainty using the method of moments in combination with the first-order upwind scheme as shown in figure 8a. Increasing the mass creates a steeper source term which leads to the same issues we reported on for the single source above. Again, we are able to capture the mean value, \bar{u} accurately but not the second moment.

Using the spectral method results in the same improvements over the upwind scheme in the prediction of the uncertainty as shown in figure 8b. The results show a more accurate detailed structure of the uncertainty bounds. Small oscillations are again observed because of numerical dispersions.

5.3 Euler equation with multiple particles

For a more challenging test problem, we consider the Euler equations with multiple particles. In addition to the singularity challenges that were present in the EL systems of the advection equation, the nonlinear Euler equations have inherent shock singularities even when the initial conditions are smooth. This further complicates uncertainty prediction.

Following [2], the particle cloud consists of 4300 particles that are uniformly distributed at $[0, 0.2981]$. The particle response time and density are $\tau_p = 3.9296 \times 10^3$ and a non-dimensional density of $\rho_p = 1200$, respectively. We set the Reynolds number to be $Re = 1.7638 \times 10^6$. We use 600 grid points to discretize the domain. We assume that the correction factor follows a Gaussian distribution with a 20% error. The mean value is determined following equation (4).

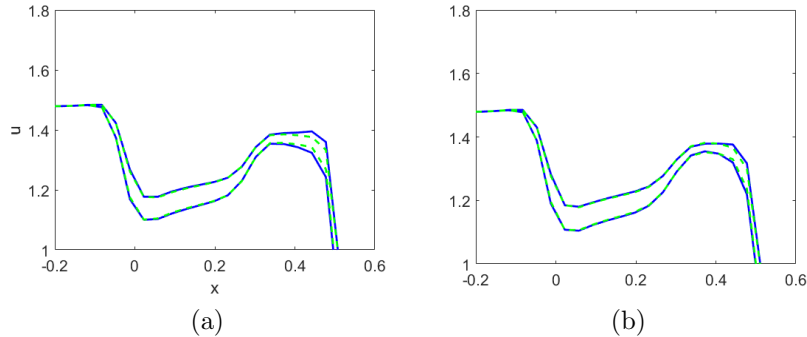


Figure 9: Two std uncertainty bounds of the fluid velocity at time $t = 0.25$ as predicted from the averaged equations (blue line) and MC simulations (dashed green line) for shock Mach number $Ma = 2$. (a) using no filtering (b) using filtering

We take the MC simulations results to be the ground truth. We report results at time, $t=0.25$ for two different shock Mach numbers: $Ma_s = 2$ in figure 9 and $Ma_s = 3$ in figure 10. At this time the shock has passed through the particles. A reflection shock is also observed ahead of the cloud. The maximum uncertainty occurs at the location of the reflected shock and slightly decreases downstream.

We are able to capture accurately the uncertainty bounds using our moment equations compared to the MC simulations. The only area where there is a mismatch is at the location of moving shock. We find it is a localized effect that depends on the strength of the shock. This is evident if we compare the predictions for the two different Mach numbers in figure 9 and figure 10. In equation (13) we see that most of the right hand side terms depend on the gradients of quantities. At the location of the shock these terms become increasingly singular and lead to singular sources in the equation for u'' . Just like for the advection case, this renders the moment equation solution inaccurate. For this compressible flow case, however, we are already using an accurate fifth-order WENO scheme, which should prevent the severe dissipation issues noted for the advection equation. Moreover, switching to the spectral method is not an option since the inherent shock wave cannot be accurately captured with a spectral method. Gibbs phenomena not only lead to inaccuracies but also lead to instability of the solution.

Instead, to reduce the impact of the moving shocks we choose to filter the shock and smoothen the solution at the shock location to improve our results. Indeed, as shown in figure 9 and figure 10 this alleviates the large numerical uncertainty at the shock front.

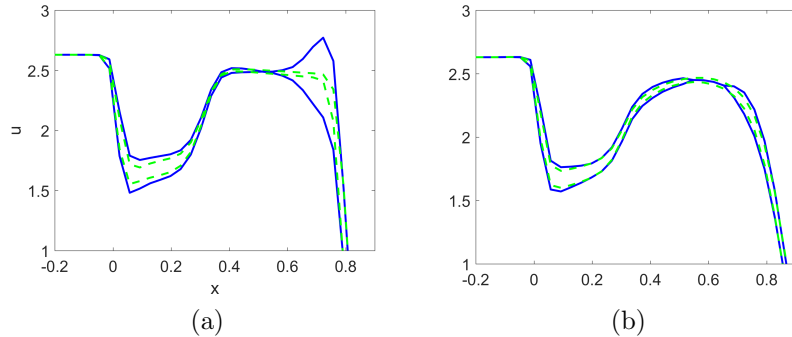


Figure 10: Two std uncertainty bounds of the fluid velocity at time $t = 0.25$ as predicted from the averaged equations (blue line) and MC simulations (dashed green line) for shock Mach number $Ma = 3$. (a) using no filtering (b) using filtering

6 Conclusions

A method of moments is developed to quantify uncertainty in Eulerian-Lagrangian models for particle-laden flows. The method is based on averaging of the deterministic equations with a stochastic forcing. We consider EL models with an Eulerian model that is governed by either the advection or Euler equations.

Comparison of Monte-Carlo simulations with the moment equations closed a priori show that the mean and variance are accurately predicted by the moment model.

If the particle sourcing is large, because of clustering of particles or because of a relatively high particle mass, strong singular sources appear in the moment equations. The singularities are caused directly by the particle sourcing itself, but also indirectly through strong fluctuations in the stochastic Eulerian solution that in turn appear in the source terms of the second moment equation and they have a greater effect. The singular source terms generate significant uncertainty.

Similarly, (singular) shock waves in the compressible particle-laden flows generate singular sources in the second moment equation and lead to high uncertainty in shocked areas.

The singular sources in the moment equations require attention if solved numerically. In the presence of smooth sources, low-order methods are adequate to solve accurately the moment equations. However, for singular sources the low-order schemes are too dissipative to obtain a reasonable match between Monte-Carlo and the moment equations. A spectral method improved this match for the linear advection equation. For the non-linear Euler equation a smoothing through filtering is necessary to be able to obtain a good comparison between the two approaches.

Our current efforts focus on the closure of the stochastic equations in a multi-scale framework. This can be achieved either by creating meta-models using mesoscale simulations in combination with common closure techniques such as gradient models.

Acknowledgments

We gratefully acknowledge the financial support by the Air Force of Scientific Research under grant number FA9550-16-1-008 and National Science Foundation NSF-CBET Award no. 1603326.

References

- [1] C. T. Crowe, M. P. Sharma, D. E. Stock, The particle-source-in cell (psi-cell) model for gas-droplet flows, *Journal of fluids engineering* 99 (2) (1977) 325–332.
- [2] G. B. Jacobs, W. Don, A high-order weno-z finite difference based particle-source-in-cell method for computation of particle-laden flows with shocks, *Journal of Computational Physics* 228 (5) (2009) 1365–1379.
- [3] G. B. Jacobs, W. Don, T. Dittmann, High-order resolution eulerian–lagrangian simulations of particle dispersion in the accelerated flow behind a moving shock, *Theoretical and Computational Fluid Dynamics* 26 (1-4) (2012) 37–50.
- [4] G. G. Stokes, On the effect of the internal friction of fluids on the motion of pendulums, Vol. 9, Pitt Press Cambridge, 1851.
- [5] V. Boiko, S. Poplavskii, Drag of nonspherical particles in a flow behind a shock wave, *Combustion, Explosion and Shock Waves* 41 (1) (2005) 71–77.
- [6] E. Loth, Compressibility and rarefaction effects on drag of a spherical particle, *AIAA journal* 46 (9) (2008) 2219–2228.
- [7] G. Tedeschi, H. Gouin, M. Elena, Motion of tracer particles in supersonic flows, *Experiments in Fluids* 26 (4) (1999) 288–296.
- [8] Z. G. Feng, E. E. Michaelides, Drag coefficients of viscous spheres at intermediate and high reynolds numbers, *Journal of Fluids Engineering* 123 (4) (2001) 841–849.
- [9] O. Sen, S. Davis, G. Jacobs, H. Udaykumar, Evaluation of convergence behavior of metamodeling techniques for bridging scales in multi-scale multi-material simulation, *Journal of Computational Physics* 294 (2015) 585–604.

- [10] O. Sen, N. J. Gaul, K. Choi, G. Jacobs, H. Udaykumar, Evaluation of kriging based surrogate models constructed from mesoscale computations of shock interaction with particles, *Journal of Computational Physics* 336 (2017) 235–260.
- [11] D. Venturi, D. M. Tartakovsky, A. M. Tartakovsky, G. E. Karniadakis, Exact pdf equations and closure approximations for advective-reactive transport, *Journal of Computational Physics* 243 (2013) 323–343.
- [12] P. Wang, D. M. Tartakovsky, Uncertainty quantification in kinematic-wave models, *Journal of computational Physics* 231 (23) (2012) 7868–7880.
- [13] R. L. Iman, W. Conover, Small sample sensitivity analysis techniques for computer models. with an application to risk assessment, *Communications in statistics-theory and methods* 9 (17) (1980) 1749–1842.
- [14] M. B. Giles, Multilevel monte carlo path simulation, *Operations Research* 56 (3) (2008) 607–617.
- [15] R. G. Ghanem, P. D. Spanos, Stochastic finite element method: Response statistics, in: *Stochastic finite elements: a spectral approach*, Springer, 1991, pp. 101–119.
- [16] D. Xiu, G. E. Karniadakis, The wiener–askey polynomial chaos for stochastic differential equations, *SIAM journal on scientific computing* 24 (2) (2002) 619–644.
- [17] X. Wan, G. E. Karniadakis, An adaptive multi-element generalized polynomial chaos method for stochastic differential equations, *Journal of Computational Physics* 209 (2) (2005) 617–642.
- [18] X. Wan, G. E. Karniadakis, Multi-element generalized polynomial chaos for arbitrary probability measures, *SIAM Journal on Scientific Computing* 28 (3) (2006) 901–928.
- [19] I. Babuška, F. Nobile, R. Tempone, A stochastic collocation method for elliptic partial differential equations with random input data, *SIAM Journal on Numerical Analysis* 45 (3) (2007) 1005–1034.
- [20] X. Ma, N. Zabaras, An adaptive hierarchical sparse grid collocation algorithm for the solution of stochastic differential equations, *Journal of Computational Physics* 228 (8) (2009) 3084–3113.
- [21] C. E. Rasmussen, Gaussian processes in machine learning, in: *Advanced lectures on machine learning*, Springer, 2004, pp. 63–71.
- [22] I. Bilonis, N. Zabaras, Multi-output local gaussian process regression: Applications to uncertainty quantification, *Journal of Computational Physics* 231 (17) (2012) 5718–5746.

- [23] V. Boiko, V. Kiselev, S. Kiselev, A. Papyrin, S. Poplavsky, V. Fomin, Shock wave interaction with a cloud of particles, *Shock Waves* 7 (5) (1997) 275–285.
- [24] J.-P. Suarez, G. B. Jacobs, W.-S. Don, A high-order dirac-delta regularization with optimal scaling in the spectral solution of one-dimensional singular hyperbolic conservation laws, *SIAM Journal on Scientific Computing* 36 (4) (2014) A1831–A1849.
- [25] J.-P. Suarez, G. B. Jacobs, Regularization of singularities in the weighted summation of dirac-delta functions for the spectral solution of hyperbolic conservation laws, *Journal of Scientific Computing* 72 (3) (2017) 1080–1092.
- [26] J. D. Schwarzkopf, M. Sommerfeld, C. T. Crowe, Y. Tsuji, *Multiphase flows with droplets and particles*, CRC press, 2011.
- [27] B. Wissink, G. Jacobs, J. Ryan, W. Don, E. van der Weide, Shock regularization with smoothness-increasing accuracy-conserving dirac-delta polynomial kernels, *Journal of Scientific Computing* (2018) 1–18.
- [28] G. Jacobs, J. S. Hesthaven, High-order nodal discontinuous galerkin particle-in-cell method on unstructured grids, *Journal of Computational Physics* 214 (1) (2006) 96–121.
- [29] H. Abe, N. Sakairi, R. Itatani, H. Okuda, High-order spline interpolations in the particle simulation, *Journal of computational physics* 63 (2) (1986) 247–267.